EFFICIENT AND ACCURATE ENCLOSURE RADIATION CONCEPTS FOR FINITE ELEMENT CODES

by

Mike Chainyk
The MacNeal-Schwendler Corporation

Three dimensional heat transfer with enclosure radiation requires the calculation of surface to surface geometric view factors. View factors for diffuse emitters and reflectors are traditionally developed by evaluating area or line integral equations for every pair of surfaces which see each other. An N surface enclosure can have N^2 unique view factors. Employing reciprocity and summation rules as many as N(N-1)/2 view factors may require calculation. If the surfaces are convex or flat, N of these view factors from a surface to itself are eliminated and the number of view factors to be calculated reduces to N(N-3)/2.

As the conduction and perhaps thermal stress analysis portion of the structure becomes more finely zoned, increasing numbers of enclosure radiation surfaces result. Finite element view factor modules are, as a consequence, notorious for large total CPU usage. This is at least partially due to their origins lying outside the finite element field (finite-difference or resistive network methods) where fewer total surfaces and directly lumped nodal heat loads persist. The approach developed in this paper applies the concepts of Gaussian integration and isoparametric finite element theory to direct determination of area weighted pseudo view factors and resultant net radiation heat loads for application to respective nodes of the finite element enclosure. Improved accuracy and reduced total computation time are expected when operating in the context of a finite element environment.

The initial problem to be solved for an enclosure radiation analysis is the determination of the geometric black-body view factor between all participating surfaces. Equation 1a is the governing area integral equation and using Stokes Theorem, Equation 1b is the corresponding contour integral equation (Reference 1).

$$F_{IJ} = \frac{1}{A}\int_{A_I}\int_{A_J}\frac{\cos\beta_I \cos\beta_J \, dA_I \, dA_J}{\pi r^2} \tag{1a}$$

$$F_{IJ} = \frac{1}{2\pi A_I}\oint_{C_I}\oint_{C_J}\left(\ell n r dx_I \, dx_J + \ell n r dy_I \, dy_J + \ell n r dz_I \, dz_J\right) \tag{1b}$$

In all but the most trivial cases these equations must be evaluated numerically. The standard methods of dual area and contour summation are indicated in their approximate numerical forms in Equations 2 and 3 (see Figure 1 for symbol definitions). Both methods generally improve in accuracy as n and subsequently the total amount of computation time increases. Computation time is approximately proportional to n^2.

$$F_{I\text{-}J} \cong \frac{1}{A_I} \sum_{I=1}^{n} \sum_{J=1}^{n} \frac{\cos\beta_I \cos\beta_J A_I A_J}{\pi r_{IJ}^2} \tag{2}$$

$$F_{I\text{-}J} \cong \frac{1}{2\pi A_I} \sum_{I=1}^{n} \sum_{J=1}^{n} \ell n r_{IJ}\, \vec{V}_I \cdot \vec{V}_J \tag{3}$$

Consider two arbitrary quadrilateral element surfaces in three dimensional space (Figure 2) which represent two solid element surfaces bounding a radiation enclosure region. Extending the isoparametric notion, the interpolation function is used in the development of a local position vector for each surface in natural coordinates. Table 1 lists the interpolation functions chosen, the developed position vector, and various vector identities necessary for defining Equation 1 in terms of elemental natural coordinates (Equation 4). Equation 5 provides the computational equivalent of Equation 2 when two-dimensional Gaussian integration is used to evaluate the integrals of Equation 4.

$$F_{I\text{-}J} = \frac{1}{A_I} \int_{-1}^{1}\int_{-1}^{1}\int_{-1}^{1}\int_{-1}^{1} \frac{\left\{\left(\frac{\partial \vec{r}}{\partial \xi} \times \frac{\partial \vec{r}}{\partial \eta}\right) \cdot \vec{R}_{I\text{-}J}\right\} \cdot \left\{\left(\frac{\partial \vec{r}'}{\partial \xi'} \times \frac{\partial \vec{r}'}{\partial \eta'}\right) \cdot \vec{R}_{J\text{-}I}\right\}}{\pi \left|R_{I\text{-}J}\right|^4} d\xi d\eta d\xi' d\eta' \tag{4}$$

$$F_{I\text{-}J} = \frac{1}{A_I} \sum_{\ell_1=1}^{\ell_{max}} \sum_{\ell_2=1}^{\ell_{max}} W_{\ell_1} W_{\ell_2} \frac{\left\{\left(\frac{\partial \vec{r}}{\partial \xi} \times \frac{\partial \vec{r}}{\partial \eta}\right) \cdot \vec{R}_{I\text{-}J}\right\} \cdot \left\{\left(\frac{\partial \vec{r}'}{\partial \xi'} \times \frac{\partial \vec{r}'}{\partial \eta'}\right) \cdot \vec{R}_{J\text{-}I}\right\}}{\pi \left|R_{I\text{-}J}\right|^4} \tag{5}$$

where $\vec{R}_{I\text{-}J}, \vec{R}_{J\text{-}I}, \frac{\partial \vec{r}}{\partial \xi}, \frac{\partial \vec{r}}{\partial \eta} \rightarrow f(\ell_1, \ell_2)$

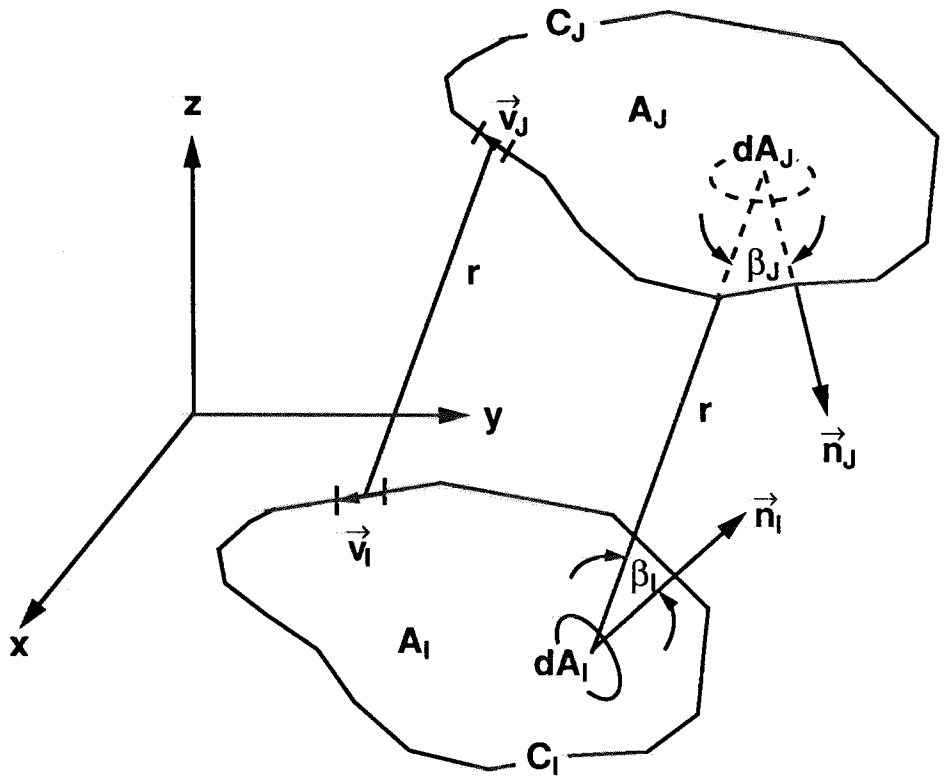

A_I and A_J are diffuse emitters and reflectors

A_I and A_J are black

A_I and A_J are isothermal

Figure 1. Arbitrary Enclosure Radiation Surfaces.

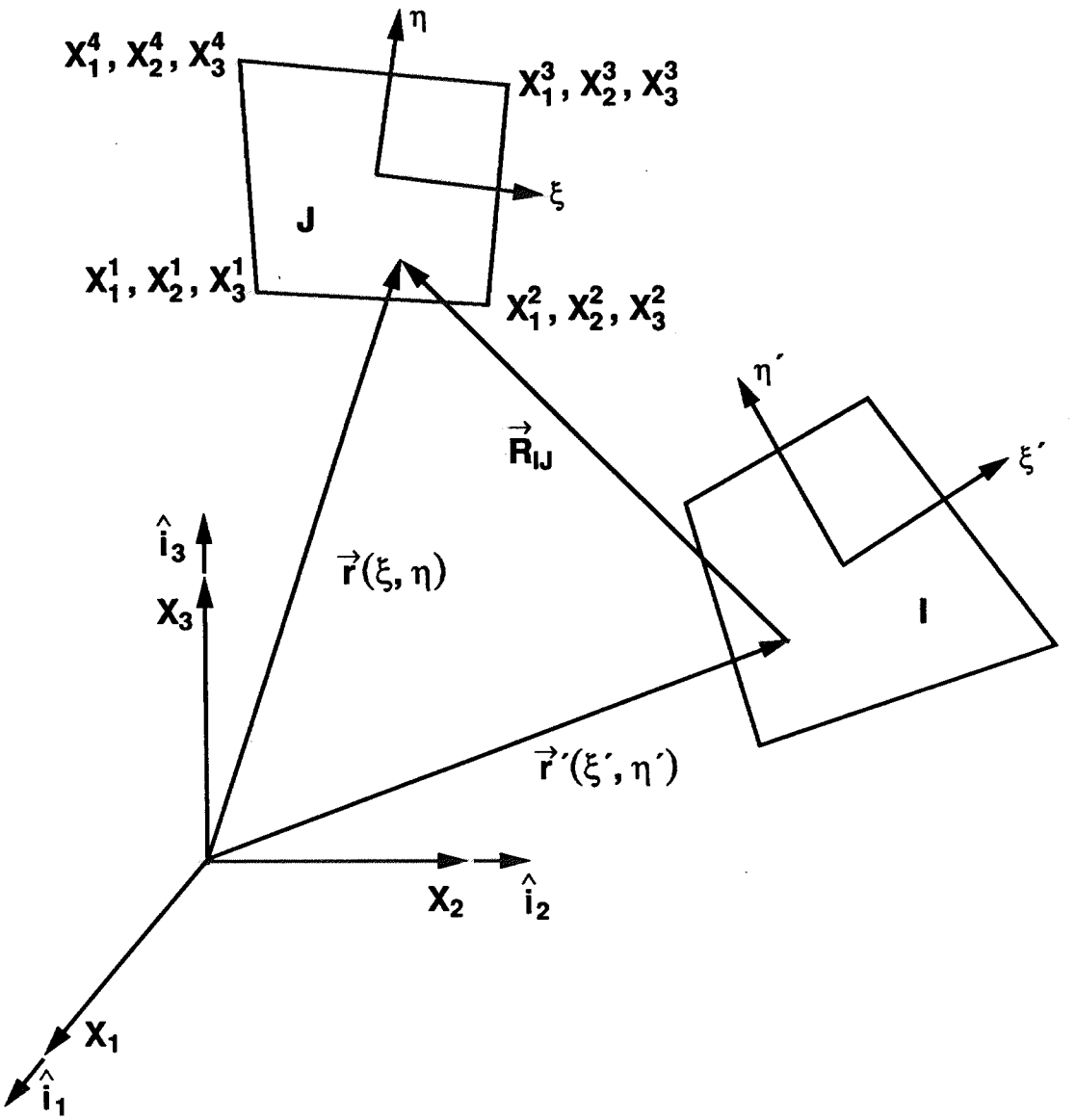

$$\vec{R}_{IJ}(\xi, \eta, \xi', \eta') = \vec{r}(\xi, \eta) - \vec{r}'(\xi', \eta')$$

Figure 2. Quadrilateral Enclosure Surfaces.

Table 1. Relations Used in the Development of Equations 4 and 5.

Calculation	Relations
Position Vector	$\vec{r}(\xi,\eta) = f_1(\xi,\eta)\,\vec{i}_1 + f_2(\xi,\eta)\,\vec{i}_2 + f_3(\xi,\eta)\,\vec{i}_3$ where $f_i(\xi,\eta) = \sum_{j=1}^{4} \phi_j X_i^j$ $X_i^j \equiv$ nodal coordinate of j^{th} node in i^{th} direction
Interpolation Functions	$\phi_j = \frac{1}{4}(1 + \xi\xi_j)(1 + \eta\eta_j)$ where $\xi_j, \eta_j \rightarrow \pm 1$
Surface Jacobian	$\lvert\underset{\sim}{J}\rvert = \left\lvert \frac{\partial\vec{r}}{\partial\xi} \times \frac{\partial\vec{r}}{\partial\eta} \right\rvert = (EG - F^2)^{\frac{1}{2}}$ where $E = \frac{\partial\vec{r}}{\partial\xi} \cdot \frac{\partial\vec{r}}{\partial\xi}$ $F = \frac{\partial\vec{r}}{\partial\xi} \cdot \frac{\partial\vec{r}}{\partial\eta}$ $G = \frac{\partial\vec{r}}{\partial\eta} \cdot \frac{\partial\vec{r}}{\partial\eta}$
Surface Normal	$\vec{n} = \lvert\underset{\sim}{J}\rvert^{-1} \left(\frac{\partial\vec{r}}{\partial\xi} \times \frac{\partial\vec{r}}{\partial\eta} \right)$
Miscellaneous	$R_{IJ} = \vec{r}(\xi,\eta) - \vec{r}(\xi',\eta')$ $\cos\beta_I = \vec{n}_I \cdot \vec{R}_{I-J}$ $ds = \lvert\underset{\sim}{J}\rvert d\xi d\eta$

L-max defines the desired order of integration. For second order Gaussian integration, L-max = 4 and the integration points and weighting functions are listed in Table 2. Equivalent data for higher order integration is available in standard texts (Reference 2). Experimental codes have been written for second, third, and fourth order integrations (LMAX = 4, 9, and 16).

Table 2. Integration Points and Weighting Factors for Second Order Gaussian Integration.

ℓ	η	ξ	W
1	$\frac{1}{\sqrt{3}}$	$\frac{1}{\sqrt{3}}$	1.0
2	$\frac{1}{\sqrt{3}}$	$\frac{-1}{\sqrt{3}}$	1.0
3	$\frac{-1}{\sqrt{3}}$	$\frac{-1}{\sqrt{3}}$	1.0
4	$\frac{-1}{\sqrt{3}}$	$\frac{1}{\sqrt{3}}$	1.0

Similarly, Equation 1b can be rewritten to take advantage of Gaussian integration for evaluating the line integrals. An experimental code utilizing one dimensional second order Gaussian integration per element edge contour has been developed. Contour integration methods are more accurate than area integral methods when the distance between surfaces is small relative to a characteristic dimension of the surface.

The second issue in the analysis of an enclosure radiation problem involves determining the net radiative heat flux to every surface of the enclosure then solving the conduction problem. This requires iteration due to the (nonlinear) surface temperature dependence of these heat flux terms. Equations 6 and 7 provide the link between surface temperature, view factor, surface properties, and enclosure net radiative heat flux.

$$B_I = \varepsilon_I \sigma T_I^4 + (1 - \varepsilon_I) \sum_{J=1}^{N} B_J F_{I-J} \qquad (6)$$

where $I = 1 \rightarrow N$

$$q_{I_{net}} = \frac{\varepsilon_I}{\rho_I}\left(\sigma T_I^4 - B_I\right) \tag{7}$$

where $B_I \rightarrow$ radiosity

$q_I \rightarrow$ net radiative heat flux at surface I

$N \rightarrow$ number of enclosure radiation surface

The derivation and solution of these equations in matrix form is detailed in Reference 3 and is not included here. The standard calculation process provides an average per unit area heat flux for every surface as a function of local temperature. The heat load must be area corrected and divided among the elements nodes for use with the finite element method. Historically, codes which used view factor Equations 2 and 3, represented a surface with a single node (by virtue of their formulation) and, as a result, weighting the heat flux for an elemental area to surrounding nodes was not necessary.

To fully exploit the Gaussian integration view factor process, consider a pseudo view factor for each integration point on every surface in its natural coordinate system (Equation 8).

$$A_i F_{i-J} = W_{\ell_i} \sum_{\ell_2=1}^{\ell_{max}} W_{\ell_2} \frac{\left\{\left(\frac{\partial \vec{r}}{\partial \xi} \times \frac{\partial \vec{r}}{\partial \eta}\right) \cdot \vec{R}_{I-J}\right\} \cdot \left\{\left(\frac{\partial \vec{r}'}{\partial \xi'} \times \frac{\partial \vec{r}'}{\partial \eta'}\right) \cdot \vec{R}_{J-I}\right\}}{\pi \left|R_{I-J}\right|^4} \tag{8}$$

where $i \rightarrow$ a discrete integration point on surface I

Correspondingly, Equations 6 and 7 may be rewritten based on integration point associated areas, radiosities, emissivities and temperatures. For two dimensional surfaces, the Jacobian of the transformation controls the magnification of area elements between the physical and natural coordinate planes. With each quadrant of the element in the natural coordinate plane having dimensions $d\xi = d\eta = 1.0$, the corresponding area in the physical plane is $|J|$. F_{i-J} and A_i (where i represents an integration point on surface I) are calculated directly about each integration point and the heat flux loads to be applied to the element nodes require no further weighting. Finally, the linearization of T^4, Equation 9, yields Equation 10 where $\hat{T}_i$ is the integration point temperature from the last iteration.

$$T_i^4 = 4\hat{T}_i^3 T_i - 3\hat{T}_i^4 \tag{9}$$

$$q_i = \frac{\varepsilon_i}{\rho_i}\left(4\hat{T}_i^3 \sigma T_i - 3\sigma\hat{T}_i^4 - B_i\right) \tag{10}$$

The first term on the right contributes to the conductance matrix while the second and third terms contribute to the load vector in the finite element assembled system equations. Iteration is performed until an acceptable level of convergence has been reached.

Several subroutines have been written to investigate expected accuracies and efficiencies of view factor calculations based on this approach for enclosure radiation analysis. Results indicate that even for only second order Gaussian integration, many view factors are found to be calculated more accurately than with area or contour summation integration utilizing significant numbers of subdivisions and operations. The dimension of the number of summations squared $\left(n^2\right)$ provides a reasonable estimate of the operation count. The notion of reduced total computation time for the entire iterative thermal analysis remains to be investigated. The perception of accuracy, regarding view factors and automatic area weighting for pseudo view factors, is expected to reduce the total number of iterations necessary for acceptable temperature convergence. This is particularly important if emissivities are a function of temperature, since Equation 6 involves the solution of a large system of simultaneous equations (i.e., matrix inversion) and will need to be resolved for every iteration.

Tables 3 and 5 provide data on this method of analysis for view factor solutions using 2nd, 3rd, and 4th order Gaussian area integrations and compares the results with the analytic solution. Tables 4 and 6 list the results of 2nd order Gaussian contour integration for the same geometries. Table 7 is a view factor calculation included for comparison and was performed with the dual area summation process currently available in the VIEW module of MSC/NASTRAN. The proposed process is seen to perform admirably.

Future work with this process, prior to its inclusion in MSC/NASTRAN, should include developing rapid methods for selecting acceptable integration order as surfaces approach one another, a further reduced order of integration (single-point quadrature) for distant surfaces, higher order Gaussian quadrature contour integration, and efficient calculation of "integration point" pseudo view factors when third surface shadowing is in effect based on detecting integration point to integration point vector intersection with a third surface.

References

1. Thermal Radiation Heat Transfer, Siegel & Howell, 2nd Ed., Hemisphere Publishing Corp., N.Y., 1981.

2. Finite Element Procedures in Engineering Analysis, Klaus-Jürgen Bathe, Prentice Hall Publishing Co., N.J., 1982.

3. Basic Heat Transfer, M. Necati Özisik, McGraw Hill, Inc., 1977.

Table 3. Shape Factor Between 1 x 1 Opposed Square Plates at a Distance X Apart Using Gaussian Area Integration.

Distance	2nd Order	% Error	3rd Order	% Error	4th Order	% Error	Analytical
0.25	1.3461	113.00	0.8303	31.40	0.6993	10.600	0.6320
0.50	0.4589	10.50	0.4196	1.06	0.4164	0.289	0.4152
1.00	0.1978	-1.00	0.1999	0.05	0.1998	0	0.1998
2.00	0.0684	-0.29	0.0686	0	0.0686	0	0.0686
3.00	0.0329	-0.30	0.0330	0	0.0330	0	0.0330
4.00	0.0191	0	0.0191	0	0.0191	0	0.0191
5.00	0.0124	0	0.0124	0	0.0124	0	0.0124

Table 4. Shape Factor Between 1 x 1 Opposed Square Plates at a Distance X Apart Using Gaussian Contour Integration.

Distance	2nd Order	% Error	Analytical	Contour Summation 2 Div/Edge	% Error
.25	.6515	+3.10%	.6320	.6793	+7.50%
.50	.4151	-.02%	.4152	.4310	+3.80%
1.00	.1994	-.30%	.2000	.2039	+1.95%

Table 5. Shape Factor Between 1 X 1 Right Angle Square Plates at a Distance X Apart Using Gaussian Area Integration.

Distance	2nd Order	% Error	3rd Order	% Error	4th Order	% Error	Analytical
0.25	0.0754	-0.92	0.0759	-0.082	0.0762	-0.082	0.0328
0.50	0.0754	-0.92	0.0759	0.260	0.0762	0.130	0.0761
1.00	0.0323	-1.52	0.0328	0	0.0328	0	0.0328
2.00	0.0089	0	0.0089	0	0.0089	0	0.0089
3.00	0.0035	0	0.0035	0	0.0035	0	0.0035
4.00	0.0017	0	0.0017	0	0.0017	0	0.0017
5.00	0.0009	0	0.0009	0	0.0009	0	0.0009

Table 6. Shape Factor Between 1 x 1 Right Angle Square Plates at a Distance X Apart Using Gaussian Contour Integration.

Distance	2nd Order	% Error	Analytical	Contour Summation 2 Div/Edge	% Error
.25	.1263	+4.00%	.1214	.1327	+9.3%
.50	.0761	0	.0761	.0797	+4.7%
1.00	.0327	-.30%	.0328	.0337	+2.7%

Table 7. MSC/NASTRAN VIEW Module Comparison to the Analytic Solution Case 1 - Opposed 1 x 1 Plates Distance X Apart.

X Distance	1/Edge	%	2 Edge	%	3/Edge	%	4/Edge	%	Analytical
0.50	0.5542	33.5	0.4478	7.85	0.4283	3.16	0.4216	1.54	0.4152